27th EPS Conference on Contr. Fusion and Plasma Phys. Budapest, 12-16 June 2000 ECA Vol. **24B** (2000) 972 -975

First Measurements of Impurity Transport in the Edge of H-Mode Plasmas at ASDEX Upgrade

R. Dux, A. Geier, A. Gude, R. Neu and the ASDEX Upgrade team

MPI für Plasmaphysik, EURATOM Association, Garching, Germany

Introduction

The confinement of impurities is to a large extent determined by the transport parameters and the impurity source distribution in the plasma edge. For H-Mode plasmas the transport parameters in the edge of the confined region are dominated by anomalous processes and are temporally modulated when Edge Localized Modes(ELM) are present. In ASDEX Upgrade H-Mode discharges with type-I ELMs first investigations of the radial transport of silicon and neon in the edge region have been performed.

Experimental set-up

The evaluation of transport coefficients at the plasma edge requires density profiles with high temporal and spatial resolution. The soft X-ray (SXR) diagnostics provides the required resolution and can give impurity densities from about 1cm inside the separatrix inward. For the Si(Ne) measurements the soft X-ray cameras had 100μm (12μm) thick Be-filters resulting in a detection efficiency $>$0.5 for photons in the energy range 2.6-15 keV (1.3-15 keV). Figure 1 shows the radiative power coefficient L_Z^{sxr} folded with the spectral sensitivity of the SXR set-up with 100μm Be-filter in the case of corona ionization equilibrium. Only the line radiation of H- and He-like Si can pass the Be-filter. For electron temperatures $T_e \approx$1 keV, L_Z^{sxr} of the main impurities C and O is almost two orders of magnitudes below L_Z^{sxr} of the investigated Si. Thus, in this T_e range the SXR radiation is very sensitive to Si. e.g. allowing for trace impurity experiments with Si laser blow-off (LBO). Radial profiles of n_e have been determined from combined analysis of the Lithium beam diagnostics and DCN interferometry, while T_e is taken from the ECE radiometer and the Thomson scattering diagnostics.

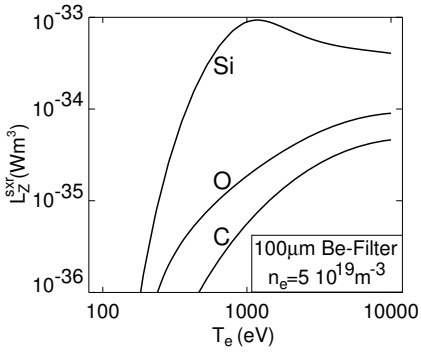

Figure 1: *Radiative power coefficients L_Z^{sxr} of Si, C and O folded with the spectral sensitivity of the SXR set-up with 100μm Be-filter in the case of corona ionization equilibrium.*

Edge SXR Profiles during an ELM Cycle

For H-Mode discharges with type-I ELMs and ELM frequency $f_{ELM} \approx$100Hz, a slow radial shift of the plasma column by ΔR=3.5cm was performed during the plateau phase of the discharge. The discharges had neutral beam heating power P_{NI}=5MW (D$\rightarrow$D$^+$), toroidal field B_T=2.5T, plasma current I_p=1.2MA, line averaged density $\bar{n}_e = 6.3 \times 10^{19}\mathrm{m}^{-3}$, safety factor q_{95}=3.3 and average triangularity δ=0.15. The radial shift of the plasma column was used to get a dense spatial grid of measurement points for T_e and SXR radiation. Measurements during many ELM cycles were overlayed by mapping onto the time difference to the start of the last ELM Δt_{ELM}.

In Figure 2 the profiles of T_e, n_e and SXR radiation flux I_{sxr} are shown versus the radial distance of the flux surface to the separatrix at midplane Δx. T_e (Fig. 2a) and I_{sxr} are measured with high time resolution and are shown for a time point shortly after the ELM at Δt_{ELM}=1ms and shortly before the next ELM at Δt_{ELM}=9.5ms. The measurement of n_e is ELM averaged (Fig. 2b). The soft X-ray profiles are shown for two nearly identical discharges. Discharge #12970 was shortly after a silconization of the vessel walls and 100μm thick Be-filters were used, such that I_{sxr} is strongly dominated by radiation from Si (Fig. 2c, 2e). In #13158 a constant Ne puff was applied and 12μm thick Be-filters were taken. Here, the line radiation of Ne is dominant (Fig. 2d, 2f).

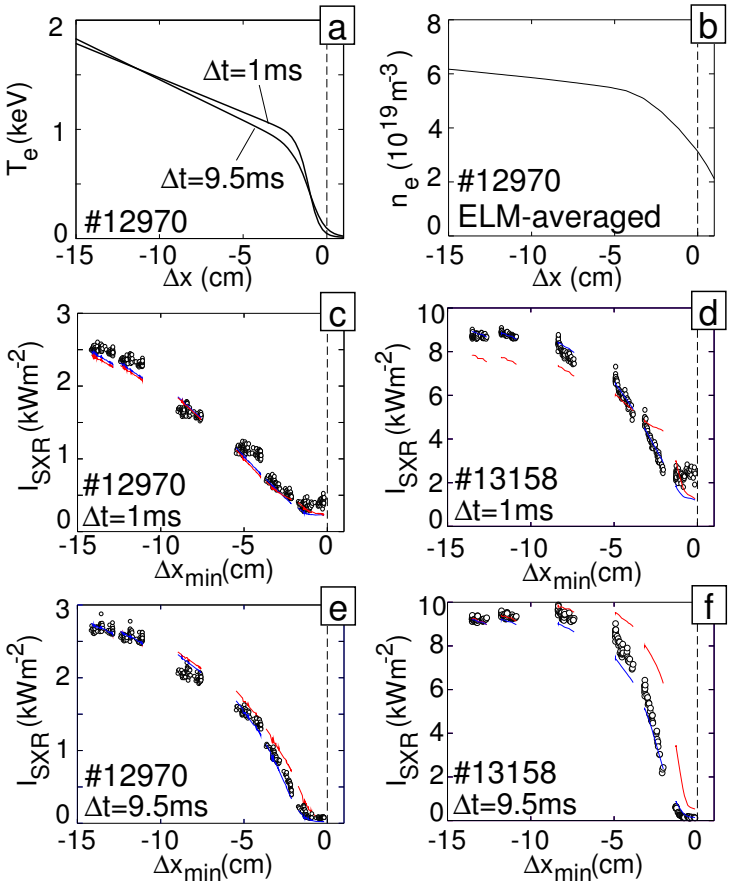

Figure 2: *T_e, n_e and SXR radiation flux I_{sxr} versus the radial distance of the flux surface to the separatrix at midplane Δx shortly after an ELM (Δt_{ELM}=1ms) and shortly before the next ELM (Δt_{ELM}=9.5ms): In discharge #12970 I_{sxr} is dominated by Si-radiation (c,e) in #13158 by Ne-radiation (d,e). The blue (model* **D***) and red lines (model* **C***) in Figures (c-e) are calculated SXR radiation fluxes assuming the two impurity transport models from Figure 3 as described in the text.*

The SXR signals are shown versus Δx_{min}, i.e. the radial coordinate of the flux surface, which is tangential to the line-of-sights at the measurement time. For both impurities, a strong modulation of I_{sxr} during an ELM cycle is observed for $\Delta x_{min} \geq -10$cm, which can not be explained by the change of T_e or n_e. This is obvious for the channels which are nearly tangent to the separatrix (compare Fig. 2c with 2e and 2d with 2f for $\Delta x_{min} \approx 0$). Here, each ELM produces a large positive spike in a plasma region with $T_e \approx 100$eV.

The temporal evolution of I_{sxr} in both discharges was used to test the relevance of two 1D models for the edge impurity transport during an ELM cycle. The features of the two models are shown in Figure 3. The generally accepted fact that each ELM leads to a loss of impurities in the confined region was the starting point of the two models. In model **D**, the ELM was assumed to cause a strong rise of the diffusion coefficient in the edge region without an outwardly directed drift velocity. Thus, the ELM can only cause a loss of the impurity content if the impurity density in the edge of the confined region develops a negative slope in the quiet phase of an ELM cycle. Since the impurity source is located outside the separatrix, an inwardly directed pinch must be present in the quiet phase. In model **C**, the transport in the quiet phase was assumed to be purely diffusive. Here, the ELM has to induce a strong outwardly directed drift velocity

to cause a loss of impurity content and a reduced rise of the diffusion coefficient in the edge region was assumed. The diffusion coefficient in the quiet phase was set equal in both models. $D(\rho_{pol})$ strongly decays from the edge to the center for $\rho_{pol}<0.85$ as was previously measured in H-mode discharges in ASDEX Upgrade [1,2]. A maximum value of D_{max}=2m^2/s was used. In the region of the edge transport barrier the diffusion coefficient was set to $D_{edge} = 0.5$m^2/s. The values of D_{max} and D_{edge} are consistent with measurements of the impurity decay times after Si-LBO in this type of discharges, however, a lower value of D_{edge} would be equally consistent, if the location of the transport barrier is moved towards the separatrix. The loss of impurity content during an ELM is ≈6% in both cases.

For both models, the impurity density distribution and the according SXR radiation during an ELM cycle were calculated with the STRAHL code [1]. The background SXR emission due to carbon was considered in both cases by using the concentration from charge exchange recombination spectroscopy (CXRS) with values of c_C ≈1%. For the discharge with Ne-Puff (#13158), 0.04% Si concentration was assumed in accordance with the emission before the start of the Ne-puff. Finally, the calculated SXR emission was integrated along the line-of-sights and the evolution of the calculated radiation fluxes was compared with the measurements of Figure 2.

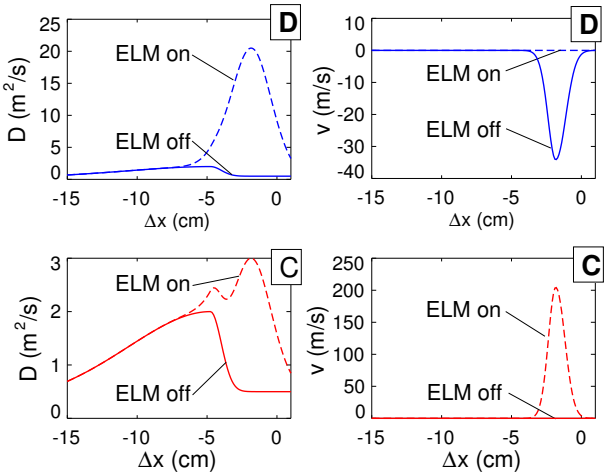

Figure 3: *Two models for the radial profiles of the diffusion coefficient D and the drift velocity v during an ELM and in between ELMs versus the radial distance of the flux surface to the separatrix at midplane Δx: In model* **D** *the ELM transport is purely diffusive with an inward pinch in between ELMs, while in model* **C** *a large outwardly directed convective transport is induced by the ELM with purely diffusive transport in between ELMs.*

The blue lines in Figure 2c-e give the results for model **D** while the red lines show the radiation fluxes for model **C**. In #12970, model **D** gives a better agreement for the profile before the ELM (2e). The results from model **C** would agree with the same profile (2e) when turning the poloidal angle of the SXR camera by 0.5^o, which is within the present uncertainty of the measured camera orientation. The profile after the ELM (Figure 2c) is equally well described by the models and the agreement gets worse when turning the camera orientation. For #13158, the differences of the two models can be seen more clearly, since He- and H-like Ne radiates at lower temperatures. Again, model **D** gives a better agreement after (Figure 2d) and before the ELM (Figure 2f). Turning of the camera by 1^o would lead to good agreement of model **C** for the profile before the ELM, however, the description of the profile after the ELM would be even worse. Thus, model **D** gives better agreement with the measurements. Further improvement of this analysis by inclusion of ELM-resolved n_e measurements and a reduced uncertainty of the camera orientation is envisaged.

ELM-averaged gradients of edge Si density

The ELM-averaged Si density gradient in the edge of type-I ELMy H-Mode discharges was determined for various pedestal densities and temperatures. For all discharges, neu-

tral beam heating power was P_{NI}=5MW (D→D$^+$) and most of the measurements result from a density scan at toroidal field B_T=2.5T, plasma current I_p=1MA and safety factor q_{95}=4 with line averaged densities in the range $\bar{n}_e$=4.4-9.0$\times 10^{19}\mathrm{m}^{-3}$. The scan was supplemented by discharges with I_p=1.2MA(0.8MA), B_T=2.5T(1.67T) and q_{95}=3.3. For discharges, which were shortly after a siliconization of the vessel walls, the Si densities at normalized poloidal flux label ρ_{pol}=0.75 could be inferred from unfolded SXR radiation fluxes. A background SXR emissivity according to 1% C concentration was used in these calculations. In a few other discharges, Si was injected with quasi continous LBO (f = 20Hz) for about 1s and the change of the SXR emissivity $\Delta\epsilon^{sxr}$ due to the LBO was used to determine the Si density.

The ELM averaged Si density in the transport barrier region was calculated from line radiation emitted by Li-like Si at λ=49.9nm (SiXII:$2p\ ^2P_{3/2} \rightarrow 2s\ ^2S_{1/2}$) which was measured on a radial line-of-sight at midplane. The calculated radial location of the emission shell of this line, i.e. $\langle\rho_{pol}(\epsilon^{lin})\rangle = \int \epsilon^{lin}\rho_{pol}dl / \int \epsilon^{lin}dl$, is depicted in Figure 4 versus T_e on the top of the pedestal at ρ_{pol}=0.9 ($\Delta x\approx$-5cm). It is inside the separatrix and depends on the steepness of the temperature profile in the edge transport barrier and on the transport parameters. $\langle\rho_{pol}(\epsilon^{lin})\rangle$ is shown for the two transport models from Figure 3, where a constant ELM frequency of f_{ELM}=100Hz is used (blue +: model **D**, red ×: model **C**). In model **D**, the emission shell is shifted towards the center due to the inward pinch term by $\Delta\rho_{pol}\approx$-0.05, which corresponds to $\Delta x\approx$-2.5cm.

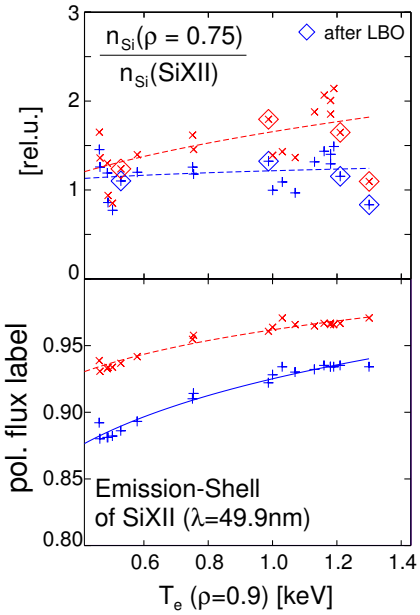

Figure 4: *Si density at ρ_{pol}=0.75 (from measured SXR profiles) divided by the Si density in the emission shell of an SiXII line versus T_e at ρ_{pol}=0.9 and calculated radial location of the emission shell (blue +: model* **D**, *red ×: model* **C**)

The upper part of Figure 4 shows the ELM-averaged ratio of the Si density at ρ_{pol}=0.75 to the density at $\rho_{pol}\geq$0.9 versus $T_e(\rho_{pol}$=0.9). Again, this ratio depends on the used transport model due to the calculated Si density from the VUV-line. The differences become most pronounced for the steepest T_e edge profiles, i.e. at high $T_e(\rho_{pol}$=0.9). Both models do not yield a large change in the impurity density ratio. For model **D**, which showed better agreement with the measurements in the previous section, the form of the edge impurity profiles seems to be independent of the pedestal temperature. However, measurements of the exact position and width of the SiXII emission shell would be needed to reduce the uncertainties in the evaluation procedure and to get a conclusive result. We plan to measure the emission profile of the SiXII line using a spectrometer which is equipped with a scanning mirror near the plasma edge.

References

[1] Dux, R., Peeters, A.G. et al., Nucl. Fusion **39** (1999) 1509.
[2] S. de Pena Hempel et al., Proc. of 24th EPS-Conf **21A**, 1401 (1997).